HNUE JOURNAL OF SCIENCE
Natural Sciences 2025, Volume 70, Issue 2, pp. 60-69
This paper is available online at http://hnuejs.edu.vn/ns
DOI: 10.18173/2354-1059.2025-0021

STRUCTURAL CHARACTERISTICS OF DENSIFIED SILICON NITRIDE UNDER HIGH PRESSURE: A MOLECULAR DYNAMICS STUDY

Dinh Cong Thanh[1], Nguyen Thi Thao[2] and Le Van Vinh[3,*]
[1]*Phenikaa University Nano Institute, Phenikaa University, Hanoi city, Vietnam*
[2]*Faculty of Physics, Hanoi National University of Education, Hanoi city, Vietnam*
[3]*School of Computing, Phenikaa University, Hanoi city, Vietnam*
[*]Corresponding author: Le Van Vinh, e-mail: vinh.levan@phenikaa-uni.edu.vn

Received March 3, 2025. Revised May 13, 2025. Accepted June 30, 2025.

Abstract. We used molecular dynamics (MD) simulations to investigate the structural properties of silicon nitride (Si_3N_4) at high temperatures and pressures. The Si_3N_4 models were cooled under a pressure of 75 GPa. A phase transition occurred in the temperature range of 3950 K to 3650 K. The structural characteristics of these Si_3N_4 models were analysed. At 4500 K and 4000 K, the Si_3N_4 models exhibited a disordered structure. As the temperature decreased, the nitrogen (N) atoms predominantly adopted a face-centered cubic (fcc) structure, and a significant fraction of N atoms exhibited hexagonal close-packed (hcp) and other disordered motifs. The hcp and disordered regions were interspersed among fcc sublattices with different orientations. The local entropy distribution of the atoms broadened and shifted toward lower values with decreasing temperature.

Keywords: Molecular dynamics, silicon nitride, crystal, structural properties.

1. Introduction

Silicon nitride (Si_3N_4) materials exhibit excellent mechanical and thermal properties [1], [2]. Thus, they are widely used in cutting tools, ball bearings, turbine and engine materials, and other fields. Crystalline Si_3N_4 exists in several forms under normal conditions. Both α– and Si_3N_4 have nitrogen atoms arranged in a hexagonal lattice, so the structural unit is a SiN_4 tetrahedron. The difference between them is that the β form is a slightly distorted tetrahedron relative to the α form. Interestingly, Si_3N_4 also exists in a third, denser form, γ–Si_3N_4, which has been synthesized at pressures above 15 GPa and temperatures exceeding 2000 K [3]. Spinel γ–Si_3N_4 has been fabricated from hexagonal structures by shock wave compression, and the γ–phase Si_3N_4 was found to be 80% at 4000 K and 45 GPa when using α–Si_3N_4 and copper powders as starting materials [4]. The phase transition under high pressure and temperature has been studied by Nishiyama et al. [5].

However, the pressure at which the transformation to the γ phase occurs is difficult to determine over a wide temperature range. Furthermore, the coexistence of α, β, and γ phases has been observed at 1873 K and 15.6 GPa, and a single phase of polycrystalline γ–Si_3N_4 appears above 2073 K [6].

First-principles simulations have been used to investigate the structural properties of Si_3N_4 ceramic materials [7], [8]. These simulations have elucidated why cubic Si_3N_4 adopts a spinel structure under high pressure and temperature, and they have predicted the formation of a post-spinel phase of Si_3N_4 at high pressures [9]. At the atomistic scale, MD simulations have been employed to study the structural changes and mechanical properties of β–Si_3N_4 nanoporous membranes [10]. In our previous works [11], [12], cubic Si_3N_4 samples were obtained by quenching under pressures of 45 GPa [11] and 60 GPa [12]. However, the structural characteristics of Si_3N_4 at high temperatures and pressures above 60 GPa have not yet been studied by MD simulations.

Thus, in this work, we used MD simulations to investigate the structural characteristics of Si_3N_4 at a pressure of 75 GPa and high temperatures. The Si_3N_4 model was cooled by quenching under a pressure of 75 GPa. The structural properties of the Si_3N_4 models are characterized by the radial distribution function (RDF), coordination number (CN), bond angle distribution (BAD), local entropy, and common neighbor analysis (CNA).

2. Content

2.1. Computational methods

We used MD simulations to model the Si_3N_4 sample. This sample contains 10,500 atoms, which were generated randomly with a minimum distance of 1.0 Å between neighboring atoms. This configuration was heated to 5000 K at a rate of 10^{-14} K/s and a pressure of 0 GPa. Here, the MD simulations adopted the pair potential described elsewhere [13]. This interaction potential was chosen because it is computationally efficient, yields models with moderately low coordination defects, and provides reasonable values for the enthalpy of formation [14]. We conducted the MD simulations using the Verlet algorithm with a timestep of 1 fs. Periodic boundary conditions were applied to the simulation box. After heating to 5000 K, the sample was maintained at this temperature for 100 ps. Then, a pressure of 75 GPa was applied to the simulation box, and the sample was cooled to 300 K at a rate of 10^{-13} K/s. The atomic configurations were stored at the desired temperatures for structural analysis.

The RDF was used to analyse the structure of the samples. The RDF is calculated as

$$g(r) = \frac{V}{N^2}\left\langle \sum_{i,j\neq i}^{N} \delta(r_{ij} - r) \right\rangle \tag{2.1}$$

where V is the volume of the sample and N is the number of atoms. From this RDF, we can calculate the CN as

$$CN(r) = 4\pi\rho \int_0^r r^2 g(r) dr \tag{2.2}$$

where is the density of the sample. We also calculated the local entropy-based fingerprint to distinguish the ordered structures of atoms [15]. The entropy of a molecular system is linked to its internal structure, which can be quantified by many body correlation functions [16], [17]. The entropy can be expanded in terms of these correlation functions

$$S = S_{ideal} + S_2 + S_3 + \text{higher order terms} \quad (2.3)$$

where S_{ideal} is the entropy of an ideal gas ensemble of monomers (or the one-body entropy) at the same density and temperature as the system under consideration, and S_2 and S_3 are the two-body entropy and three body entropy, respectively. The excess entropy of the system can be written as

$$S_{ex} = S - S_{ideal} \quad (2.4)$$

It is often assumed that the dominant term in a series expansion is the two-body contribution, S2, and that the remaining higher order terms can be neglected. Thus,

$$S_{ex} \cong S_2 = -2\pi\rho k_B \int_0^\infty [g(r)\ln g(r) - g(r) + 1] r^2 dr \quad (2.5)$$

where ρ is the density of the sample, and g(r) is the RDF. The analysis of $I(r)=[g(r)\ln(r)-g(r)+1]r^2$ suggests that S_2 can be used as a fingerprint to identify local structures [15]. Thus, the entropy is calculated for each atom *i* in the sample as

$$s_S^i = -2\pi\rho k_B \int_0^{r_m} \left[g_m^i(r)\ln(g_m^i(r)) - g_m^i(r) + 1 \right] r^2 dr \quad (2.6)$$

where $g_m^i(r)$ is the RDF for atom i, and r_m is an upper integration limit. The average local entropy is calculated to further clarify the distinction of the distributions as follows:

$$\bar{s}_S^i = \frac{\sum_j s_S^i f(r_{ij}) + s_S^i}{\sum_j f(r_{ij}) + 1} \quad (2.7)$$

where $f(r_{ij})$ is a switching function calculated as

$$f(r_{ij}) = \frac{1-(r_{ij}/r_a)^N}{1-(r_{ij}/r_a)^M} \quad (2.8)$$

with N = 6 and M = 12. Here, r_a is chosen as 4.2 Å for the Si_3N_4 sample. The CNA is also used to determine the crystalline structure [18].

2.2. Results and discussion

The change in volume with temperature during the cooling process is shown in Figure 1. The volume of the Si_3N_4 model decreases linearly as the temperature falls to 3950 K. Then, the volume drops abruptly between 3950 K and 3650 K, indicating a structural phase transition. As the temperature decreases further, the volume again decreases linearly. Experiments have also reported the structural phase transformation of Si_3N_4 at 4000 K under compressive pressure [4].

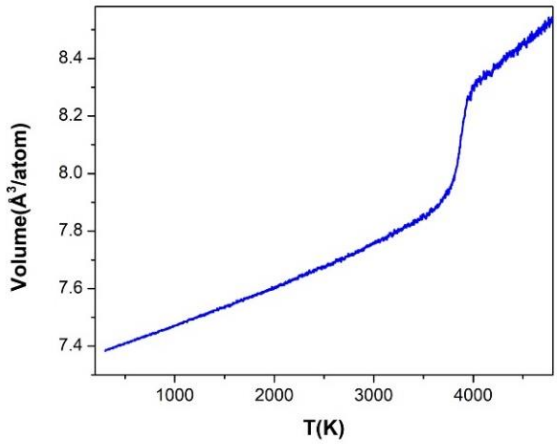

Figure 1. The volume changes with the temperature

The RDFs of the models at different temperatures are shown in Figure 2. At high temperatures (4000 K and 4500 K), the RDFs exhibit only two peaks, indicating that the models have a disordered structure. As the temperature decreases to 3500 K, additional peaks appear in the RDFs, showing that the structure becomes more ordered than at 4000 K and 4500 K. With further temperature reduction, the RDFs display even more peaks, which become sharper and higher. This indicates that the models become increasingly ordered as temperature decreases. The first peak of these RDFs corresponds to the Si–N bond length. Its position shifts gradually from 1.73 Å to 1.82 Å as the temperature decreases from 4500 K to 300 K. Experimental data also show that the Si–N bond length in amorphous Si_3N_4 is 1.729 ± 0.005 Å [19], while the tetrahedral ($Si–N_4$) and octahedral ($Si–N_6$) bond lengths in crystalline γ–Si_3N_4 are 1.7849 Å and 1.8718 Å [20], respectively. This suggests that at 4000 K and 4500 K the models resemble amorphous Si_3N_4, whereas at lower temperatures they exhibit a crystalline structure.

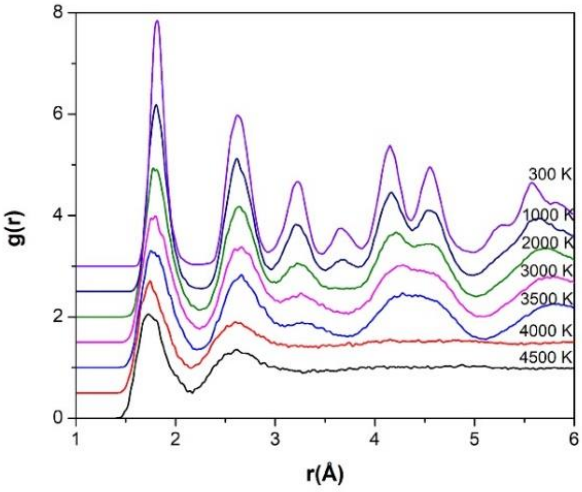

Figure 2. The RDF of the models at the different temperatures

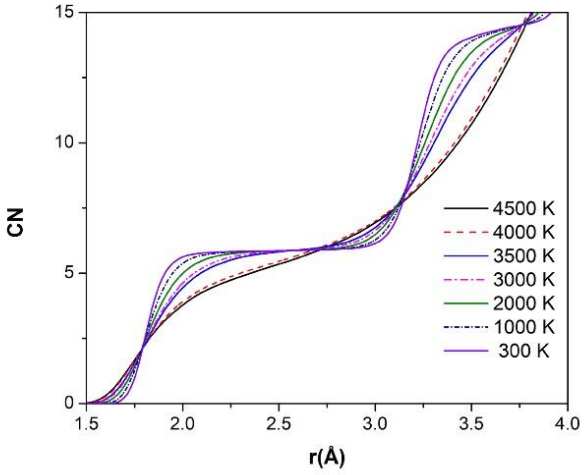

Figure 3. The CN varies with the distance at different temperatures

Figure 3 shows that the CN of the models changes with distance. At 4500 K and 4000 K, the curves increase steeply with distance, while they change in a stepwise manner at temperatures below 3500 K. In particular, the CN of the model at 300 K remains almost unchanged at approximately 5.8 in the range from 2 Å to 2.8 Å. We also examined the N–Si–N BAD of the models, as presented in Figure 4. The main peaks of the N–Si–N BADs are located at 88.5°. This peak becomes narrower and increases in height with decreasing temperature down to 300 K, indicating that structural SiN_6 units become more symmetrical. These results show that a large number of atoms are arranged in tetrahedral units at temperatures below 3500 K.

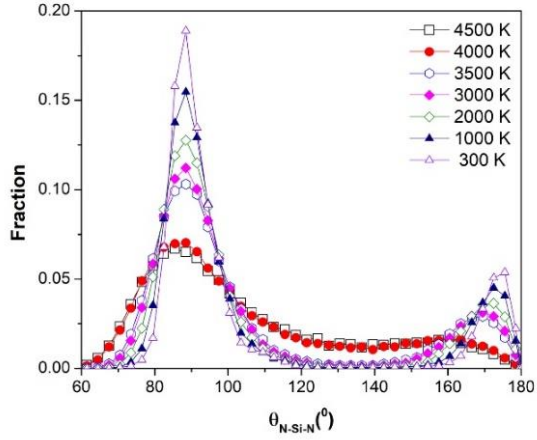

Figure 4. The N–Si–N BAD changes with decreasing temperature

Figure 5 shows the distribution of the average local entropy $\overline{S_S}$. At 4500 K, the distribution follows a normal distribution. The peak of the distribution is skewed and also shifts to the left with decreasing temperature down to 300 K. Furthermore, it also broadens with decreasing temperature. The atom with a more ordered structure has a lower $\overline{S_S}$value, and vice versa. This implies that the model at a lower temperature has

a higher ordered structure. As observed in Figure 4, we can see that there is an intersection between the distributions at 4500 K and 300 K, indicating that there are still atoms at high temperature with "solid-like structure" and atoms at low temperature with "liquid-like structure" [15]. Thus, we visualized redatoms with $\overline{S_S}$> –38.2 k_B and blue atoms with $\overline{S_S}$≤ 38 - 38.2 k_B as presented in Figure 6. Note that –38.2 k_B is the intersection point between the distributions at 4500 K and 300 K. Here we refer to the blue atoms as solid-like atoms and the red atoms as liquid-like atoms. As observed in Figure 6, the blue atoms still cluster together even at high temperatures, and the red atoms gather together into clusters with decreasing temperature.

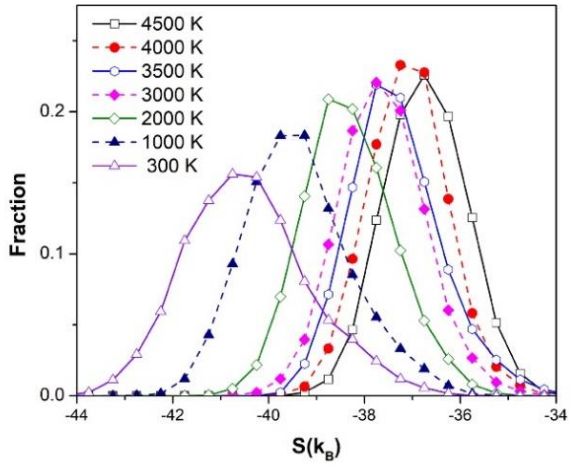

Figure 5. The distribution of average local entropy at the different temperatures

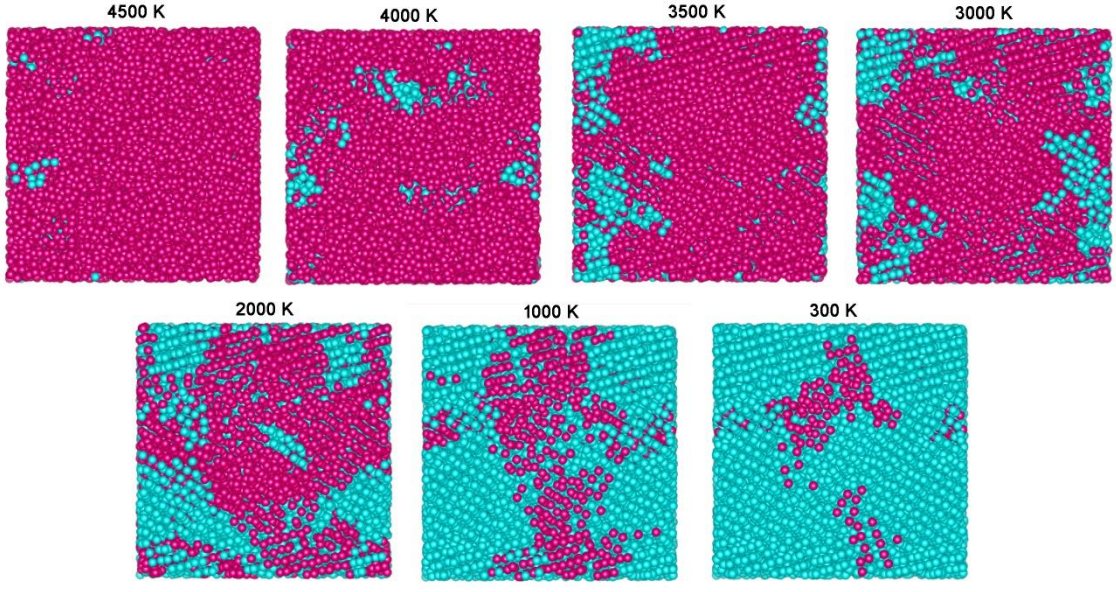

Figure 6. Visualizations of the average local entropy of atoms in the models (Red atoms with $\overline{S_S}$> –38.2 k_B and blue atoms with $\overline{S_S}$≤38 –38.2 k_B)

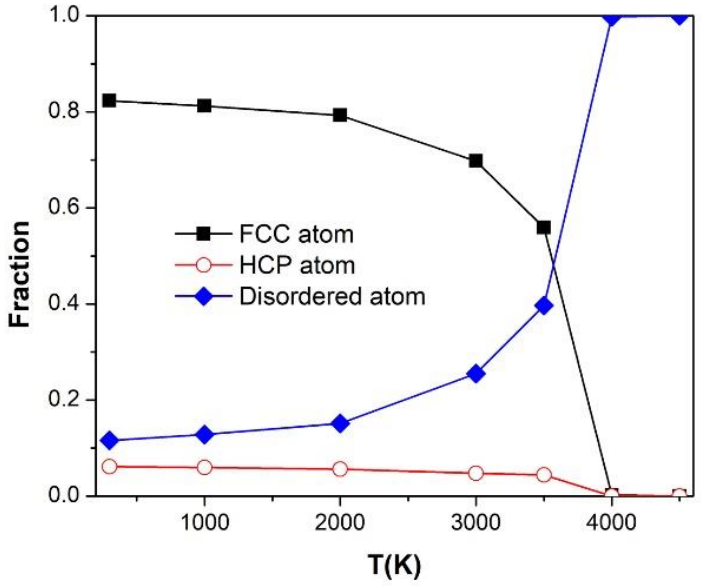

Figure 7. Fraction of fcc, hcp, and disordered atoms with decreasing temperature

We used CNA analysis to determine the crystalline structures in these models and found that N atoms form fcc and hcp lattices. Figure 7 shows the fractions of fcc, hcp, and disordered N atoms as a function of temperature. No crystalline atoms are found at 4500 K. However, 12 fcc N atoms form in the model at 4000 K. As the temperature decreases to 3500 K, many more fcc N atoms appear, along with a small number of hcp N atoms. With further cooling to 300 K, both fcc and hcp populations increase gradually.

Figure 8 shows cross sections of the models. At 4000 K, the structure is largely disordered. At 3500 K, two fcc N clusters with different orientations emerge, with hcp and disordered N atoms inserted between them. As temperature decreases, the disordered N atoms transform into fcc and hcp sites. We also calculated the average potential energy (APE) of fcc, hcp, and disordered atoms (Figure 9). The APE is lowest for fcc atoms, higher for hcp atoms, and highest for disordered atoms. This ordering obeys Ostwald's rule of stages [21], which states that phases with lower energy barriers form first. The APE gap between disordered and hcp atoms is small, whereas the gap between hcp and fcc atoms is large. Furthermore, the hcp clusters intermingle with disordered atoms inserted between two fcc clusters of different orientations (see Figure 8). Thus, disordered and hcp atoms represent defects and stacking faults within the fcc lattice, respectively.

We also found that fcc N atoms bond to Si atoms in both the SiN_6 and SiN_4 units. This fcc arrangement is similar to the mineral $MgAl_2O_4$, which crystallizes in space group Fd-3m [22]. The cubic spinel Si_3N_4 (γ–Si_3N_4) adopts an ideal spinel structure: an fcc lattice of N atoms, with Si occupying one-eighth of the interstitial SiN_4 sites and one-half of the SiN_6 sites [23]. Thus, the crystal structures of our samples closely resemble that of γ–Si_3N_4.

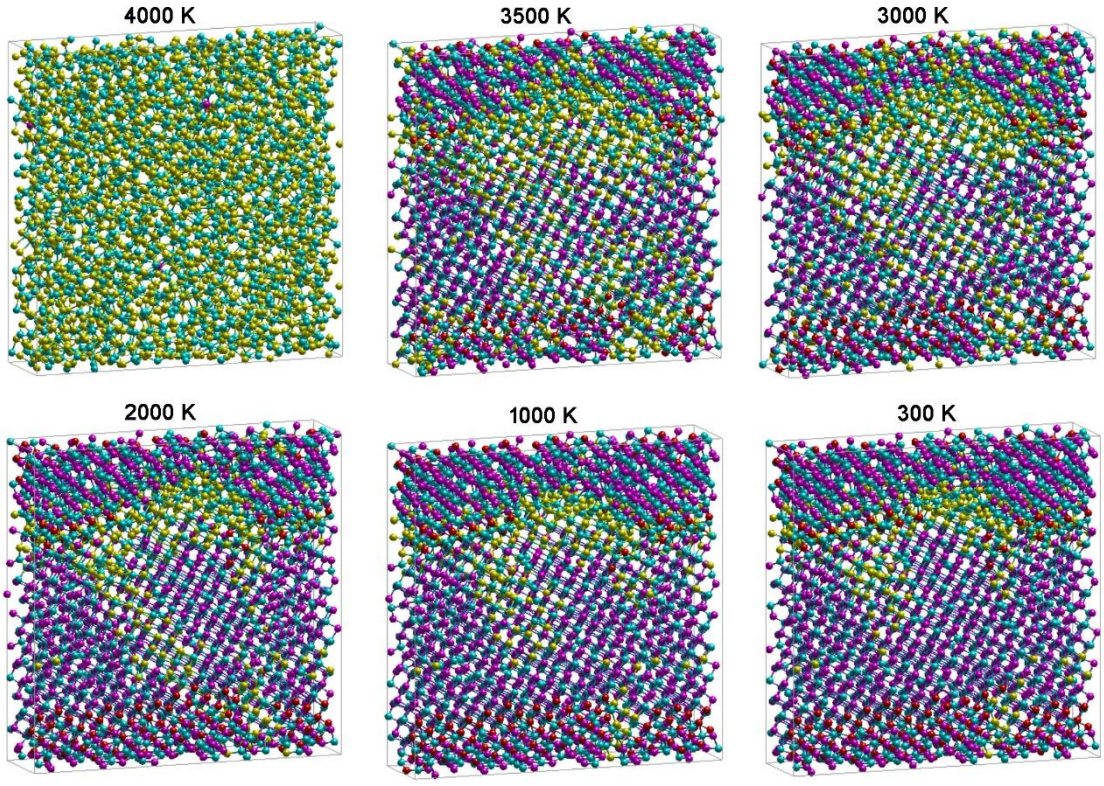

Figure 8. Cross-sectional models at the different temperatures (Cian: Si atoms, violet: fcc N atoms, red: hcp N atoms, and yellow: disordered N atoms)

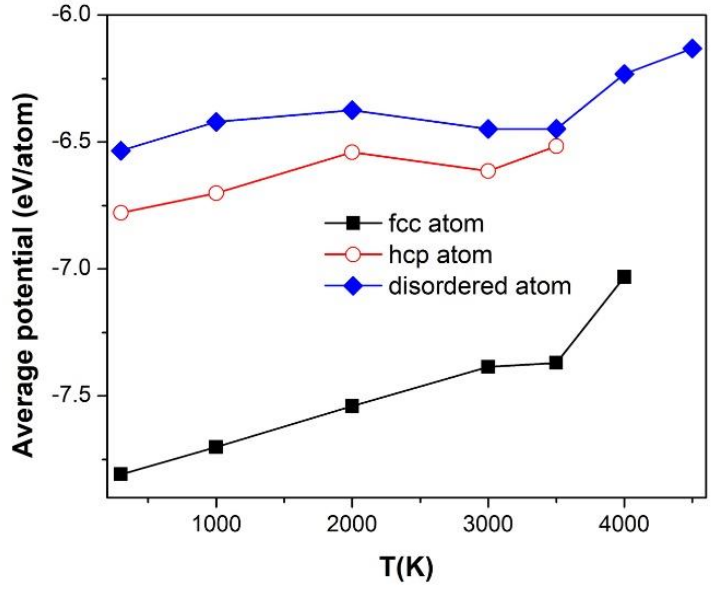

Figure 9. The APE of fcc, hcp, and disordered atoms at the different temperatures

3. Conclusions

The MD simulations were used to model the Si_3N_4 samples during the cooling process under a pressure of 75 GPa. The phase transformation from a disordered to a crystalline structure occurs in the temperature range of 3950 K to 3650 K. This phase transition obeys Ostwald's rule of stages. At 3500 K, the majority of N atoms adopt an fcc lattice forming spinel γ–Si_3N_4, while a significant fraction exhibit hcp and disordered structures. The hcp and disordered regions are intermixed at the grain boundaries of γ–Si_3N_4. With decreasing temperature, the fractions of fcc and hcp atoms increase gradually, while the fraction of disordered atoms decreases. The local-entropy analysis also shows that the model at 4500 K still contains a cluster of solid-like atoms, and the model at 300 K still contains a cluster of liquid-like atoms.

REFERENCES

[1] Sanchez-Gonzalez E, Miranda P, Guiberteau F & Pajares A, (2009). Effect of temperature on the pre-creep mechanical properties of silicon nitride. *Journal of the European Ceramic Society*, 29(12), 2635. https://doi.org/10.1016/j.jeurceramsoc.2009.03.011.

[2] Luo C, Zhang Y & Deng T, (2021). Pressureless sintering of high performance silicon nitride ceramics at 1620 °C. *Ceramics International*, 47(20), 29371-29378. https://doi.org/10.1016/j.ceramint.2021.07.104.

[3] Zerr A, Miehe G, Serghiou G, Schwarz M, Kroke E, Riedel R, Fueb H, Kroll P & Boehler R, (1999). Synthesis of cubic silicon nitride. *Nature*, 400, 340. https://doi.org/10.1038/22493.

[4] Yao H, Xu Q & Tang J, (2009). Synthesis and stability of cubic silicon nitride. *Advanced Materials Research*, 79-82, 1467. https://doi.org/10.4028/www.scientific.net/AMR.79-82.1467.

[5] Nishiyama N, Langer J, Sakai T, Kojima Y, Holzheid A, Gaida NA, Kulik E, Hirao N, Kawaguchi SI, Irifune T & Ohishi Y, (2019). Phase relations in silicon and germanium nitrides up to 98 GPa and 2400 °C. *Journal of the American Ceramic Society*, 102, 2195. https://doi.org/10.1111/jace.16063.

[6] Nishiyama N, Ishikawa R, Ohfuji H, Marquardt H, Kurnosov A, Taniguchi T, Kim BN, Yoshida H, Masuno A, Bednarcik J, Kulik E, Ikuhara Y, Wakai F & Irifune T, (2017). Transparent polycrystalline cubic silicon nitride. *Scientific Reports*, 7, 44755. https://doi.org/10.1038/srep44755.

[7] Jiang JZ, Lindelov H, Gerward L, Stahl K, Recio JM, Mori-Sanchez P, Carlson S, Mezouar M, Dooryhee E, Fitch A & Frost DJ, (2002). Compressibility and thermal expansion of cubic silicon nitride. *Physical Review B,* 65, 161202. https://doi.org/10.1103/PhysRevB.65.161202.

[8] Kiefer B, Shieh SR, Duffy TS & Sekine T, (2005). Strength, elasticity, and equation of state of the nanocrystalline cubic silicon nitride γ−Si3N4 to 68GPa. *Physical Review B*, 72, 014102. https://doi.org/10.1103/PhysRevB.72.014102.

[9] Yu BH & Chen D, (2012). Investigations of meta-stable and post-spinel silicon nitrides. *Physica B*, 407(24), 4660. https://doi.org/10.1016/j.physb.2012.09.025.

[10] Shargh AK & Abdolrahim AK, (2019). Molecular dynamics simulation of structural changes in single crystalline silicon nitride nanomembrane. *Ceramics International*, 45, 23070-23077. https://doi.org/10.1016/j.ceramint.2019.07.355.

[11] Nguyen TT, Nguyen TTH & Le VV, (2022). Structural and Mechanical Properties of Cubic Silicon Nitride: A Molecular Dynamics Study. *VNU Journal of Science: Mathematics-Physics*, 38(3), 14-23. https//doi.org/10.25073/2588-1124/vnumap.4699.

[12] Le VV, Dinh TH & Nguyen TH, (2023). Microstructural and Mechanical Properties of Cubic Silicon Nitride: Insights from Molecular Dynamics Simulation. *Journal of Materials Engineering and Performance*, 32, 9875-9883. https://doi.org/10.1007/s11665-023-07824-6.

[13] Marian CM, Gastreich M & Gale JD, (2000). Empirical two-body potential for solid silicon nitride, boron nitride, and borosilazane modifications. *Physical Review B*, 62, 3117. https://doi.org/10.1103/PhysRevB.62.3117.

[14] Dasmahapatra A & Kroll P, (2018). Modeling amorphous silicon nitride: A comparative study of empirical potentials. *Computational Materials Science*, 148, 165. https://doi.org/10.1016/j.commatsci.2017.12.008.

[15] Piaggi PM & Parrinello M, (2017). Entropy based fingerprint for local crystalline order. *The Journal of Chemical Physics,* 147, 114112. https://doi.org/10.1063/1.4998408.

[16] Voyiatzis E, Müller-PlatheMichael F & Böhm C, (2013). Do Transport Properties of Entangled Linear Polymers Scale with Excess Entropy? *Macromolecules*, 46(21), 8710-8723. https://doi.org/10.1021/ma401617z.

[17] Wallace DC, (1987). On the role of density fluctuations in the entropy of a fluid. *The Journal of Chemical Physics*, 87, 2282-2284. https://doi.org/10.1063/1.453158.

[18] Faken D & Jonsson H, (1994). Systematic analysis of local atomic structure combined with 3D computer graphics. *Computational Materials Science*, 2, 279. https://doi.org/10.1016/0927-0256(94)90109-0.

[19] Misawa M, Fukunaga T, Niihara K, Hirai T & Suzuki K, (1979). Structure characterization of CVD amorphous Si3N4 by pulsed neutron total scattering, *Journal of Non-Crystalline Solids*, 34(3), 313-321. https://doi.org/10.1016/0022-3093(79)90018-8.

[20] Jiang JZ, Stahl K, Berg RW, Frost DJ, Zhou TJ & Shi PX, (2000). Structural characterization of cubic silicon nitride. *Europhysics Letters*, 51(1). DOI 10.1209/epl/i2000-00337-8.

[21] Ten Wolde PR & Frenkel D, (1999). Homogeneous nucleation and the Ostwald step rule. *Physical Chemistry Chemical Physics*, 1(9), 2191-2196. DOI: 10.1039/A809346F.

[22] Wyckoff NW, (1962). *Crystal Structures*. Interscience, New York.

[23] Fang CM, de Wijs GA, Hintzen GA & de With G, (2003). Phonon spectrum and thermal properties of cubic Si_3N_4 from first-principles calculations. *Journal of Applied Physics*, 93, 5175. https://doi.org/10.1063/1.1566473.